Journal of Pharmaceutical Analysis 11 (2021) 191–199

Contents lists available at ScienceDirect

Journal of Pharmaceutical Analysis

journal homepage: www.elsevier.com/locate/jpa

Original article

Curcumin encapsulated dual cross linked sodium alginate/ montmorillonite polymeric composite beads for controlled drug delivery

O. Sreekanth Reddy [a], M.C.S. Subha [a, *], T. Jithendra [a], C. Madhavi [b], K. Chowdoji Rao [b]

[a] Department of Chemistry, Sri Krishnadevaraya University, Ananthapuramu, 515003, India
[b] Department of Polymer Science and Technology, Sri Krishnadevaraya University, Ananthapuramu, 515003, India

ARTICLE INFO

Article history:
Received 30 May 2019
Received in revised form
30 September 2019
Accepted 5 July 2020
Available online 4 August 2020

Keywords:
Curcumin
Sodium alginate
Montmorillonite
Microbeads
Drug delivery

ABSTRACT

The aim of the present work is fabrication of dual cross linked sodium alginate (SA)/montmorillonite (MMT) microbeads as a potential drug vehicle for extended release of curcumin (CUR). The microbeads were prepared using in situ ion-exchange followed by simple ionotropic gelation technique. The developed beads were characterized by Fourier transform infrared spectroscopy (FTIR), differential scanning calorimetry (DSC), thermogravimetric analysis (TGA), X-ray diffraction (X-RD) and scanning electron microscopy (SEM). The effect of MMT on encapsulation efficiency of CUR and intercalation kinetics was investigated. Dynamic swelling study and in vitro release study were investigated in simulated intestinal fluid (pH 7.4) and simulated gastric fluid (pH 1.2) at 37 °C. Results suggested that both the swelling and in vitro release studies were influenced by the pH of test media, which might be suitable for intestinal drug delivery. The release mechanism was analyzed by fitting the release data into Korsmeyer-Peppas equation.

1. Introduction

In today's pharmaceutical formulation, polymer based hydrogel plays a vital role in several biomedical applications. Hydrogels have many advantages over other drug carriers due to their water intake capacity, biocompatibility and biodegradability [1,2]. However, hydrogels have a few drawbacks like unrestrained release rate and non-controlled swelling properties, which lead to several side effects. To control the release rate and swelling properties of hydrogels, certain substances have been incorporated in the hydrogels such as clay minerals, surface coating with other polymers such as chitosan [3] and poly-L-lysine [4]. Controlled release drugs have many advantages over conventional forms such as reducing release rate, minimizing side effects and keeping drug concentration at effective levels in plasma.

For the last few decades, clay minerals have been extensively used in pharmaceutical formulations as lubricants, disintegrants, diluents, pigments and binders. Since ancient times, clay materials have been used to treat food poisoning, aches and pains, infections, and mineral deficiencies [5]. In recent years, researchers show much interest in montmorillonite (MMT) in pharmaceutical formulations, because of good adsorbance ability, large specific area, high cation-exchange capacity, standout adhesive ability, intercalate large molecules into the space and drug carrying capability [6]. MMT is a naturally occurring inorganic material, composed of silica tetrahedral sheets layered between alumina octahedral sheets at a ratio of 2:1, respectively [7]. MMT intercalates with drug molecules by adsorption process; during intercalation drug molecules replace the hydroxyl groups present on the outer surface and inter layer space of clay material [8]. Many researchers have reported that the mechanisms involved in the interaction between drug molecules and MMT are hydrogen bonding, ion exchange, van der Waals interaction, hydrophilic/hydrophobic interaction and so on [9–11]. Among all the mechanisms, ion exchange interactions have received considerable attention between the two components of the hybrid system [12]. Ion-exchange interaction might take place by mixing solid substrates (namely, ion exchangers) with ionic drugs in solution. In biological fluids, "counterions" can displace the drug from the substrate and deliver it into the body. The exchanger may be then eliminated or biodegraded [13].

Peer review under responsibility of Xi'an Jiaotong University.
* Corresponding author.
E-mail address: mcssubha3@gmail.com (M.C.S. Subha).

https://doi.org/10.1016/j.jpha.2020.07.002

Sodium alginate (SA) is an anionic polysaccharide comprising 1 → 4 linked β-(D)-guluronic (G) and α-(L)-mannuronic (M) acid residues arranged as -M-G- sequences randomly [14]. SA is one of the most popular anionic polymers used in biomedical applications due to its versatile properties such as biocompatibility, hydrophilicity, biodegradability, non-toxicity and good potentiality in drug delivery applications [15,16]. SA forms three-dimensional network hydrogel by electrostatic attraction between the guluronic acid residues through the exchange of sodium ions of guluronic acid with the multivalent cations such as Ca^{2+}, Mg^{2+}, Ba^{2+}, Sr^{2+} and makes egg-box structure [17]. However, the calcium alginate hydrogels have few limitations such as non-controlled swelling properties and drug release profile due to the inherent stiffness of the Ca^{2+} alginate [18]. In order to control the release rate and swelling properties, calcium alginates beads are blended with other polymers like chitosan, locust bean gum and gelatin to form a complex structure through hydrogen bonding, ion-ion, and dipole-ion interactions. A few articles have reported that MMT containing alginate polymer blend microbeads acts as good carriers for drug delivery applications [19–21].

Curcumin (CUR) (Fig. 1), an active bio-compound obtained from the yellow spice of *Curcuma longa* (Indian spice), is a natural pigment with antibacterial, antifungal antiviral, anti-inflammatory, anti-malarial, antioxidant, anti-mutagenic effects and wound healing properties, and it enhances anti-tumour activity against different types of cancer cells [22–25]. However, therapeutic use of CUR is limited due to its poor water solubility, short life and low bioavailability [26,27]. Generally simple ionotropic gelation techniques are used to encapsulate the hydrophilic drugs in hydrogel beads, but this technique gives low encapsulation efficiency of CUR due to its low water solubility. Therefore, in order to increase the drug encapsulation efficiency of CUR, MMT clay material was used in the present study; the muco-adhesiveness of MMT clay material facilitates the intercalation of drug molecules, which inturn increases the bioavailability of CUR.

In the present study, we focused on fabricating heteroionic SA/MMT beads by doping calcium-alginate matrix with different multivalent cations (Mg^{2+}, Ba^{2+} and Al^{3+}). The incorporation of multivalent ions into calcium-alginate matrix would modify swelling property and release the rate of bio-active molecules. The developed microbeads were characterized by different techniques such as Fourier transform infrared spectroscopy (FTIR), X-ray diffraction (X-RD), differential scanning calorimetry (DSC), thermo gravimetric analysis (TGA) and scanning electron microscopy (SEM). The swelling study and in vitro drug release kinetics were performed in both simulated intestinal fluid and simulated gastric fluid at 37 °C and the results are presented here.

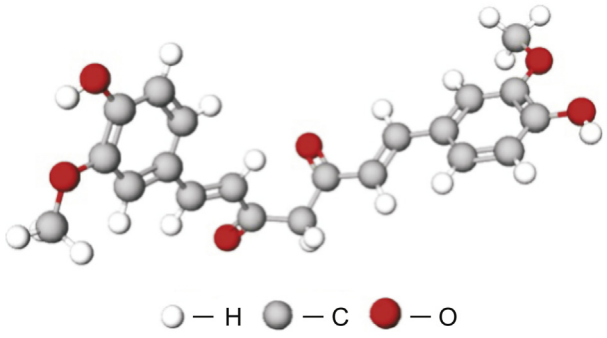

Fig. 1. Chemical structure of curcumin.

2. Experimental

2.1. Materials

MMT was purchased from Sigma–Aldrich (USA). SA and calcium chloride, magnesium chloride, barium chloride and aluminium chloride were purchased from SD Fine Chemicals, Mumbai, India. CUR was purchased from Loba Chemicals, Mumbai, India. Water used was of high purity grade after double distillation.

2.2. Preparation of SA/MMT microbeads

200 mg of SA was weighed and dissolved in water under constant stirring overnight. To this solution, 200 mg of MMT was added and stirred well. A required amount of CUR was added and stirred to obtain a homogeneous solution. Afterwards the suspension was placed in sonicator for 5 min to get homogenous suspension. The resulting suspension was slowly dropped into different ratios of $CaCl_2$, $MgCl_2$, $AlCl_3$ and $BaCl_2$ solution (as given in Table 1), where the spherical beads formed instantly were kept for 40 min. The obtained wet beads were collected by decantation, washed three times with double distilled water to remove the drug attached on the bead surface, and finally were dried in air overnight at room temperature.

2.3. Characterization methods

2.3.1. Intercalation kinetics

To estimate the maximum time required for intercalation of CUR with MMT, 50 mg of CUR and 100 mg of MMT were weighed and dissolved in 20 mL of double distilled water with continuous stirring at 37 °C. At regular intervals of time (15, 30, 60, 90, 120, 240 and 360 min), the drug solution was filtered and the concentration of CUR was assayed using UV spectrophotometer at fixed λ_{max} value of 470.00 nm.

2.3.2. Fourier transform infrared spectroscopy (FTIR)

FTIR spectra of SA, CUR, MMT, placebo microbeads, and drug loaded microbeads were measured with an FTIR spectrophotometer (model Bomem MB-3000, with Horizon MB™ FTIR software). The samples were mixed with KBr and compressed into pellets and scanned from 400 to 4000 cm^{-1} to find out the possible chemical interactions between polymers and drug.

2.3.3. Differential scanning calorimetry (DSC)

DSC curves of CUR, MMT, placebo microbeads, and drug loaded microbeads were recorded using thermogravimetry analyzer (Rheometric Scientific, Model DSC-SP, UK). The analysis was performed by heating the sample from 40 to 600 °C at the heating rate of 10 °C/min under nitrogen atmosphere.

2.3.4. Thermogravimetric analysis (TGA)

TGA of CUR, MMT, placebo microbeads, and drug loaded microbeads was carried out using thermogravimetry analyzer (Rheometric Scientific, Model DSC-SP, UK). About 5–7 mg of sample was placed into alumina crucible and the thermo grams were recorded between 40 °C to 600 °C at a heating rate of 10 °C/min under nitrogen atmosphere.

2.3.5. X-ray diffraction (X-RD)

The X-ray diffraction of CUR, placebo microbeads, and drug loaded microbeads was performed by a wide angle X-ray scattering diffractometer (Panalytical X-ray Diffractometer, model-X'pert Pro) with CuKα radiation (λ = 1.54060) at a scanning rate of 10°/min to determine the crystallinity.

Table 1
Formulation and composition of all samples used for the studies.

Formulation code	SA (mg)	MMT (mg)	CUR (mg)	Distilled water (mL)	$CaCl_2$ (%)	$MgCl_2$ (%)	$BaCl_2$ (%)	$AlCl_3$ (%)
Ca	200	200	50	20	5	0	0	0
CaMg	200	200	50	20	2.5	2.5	0	0
CaBa	200	200	50	20	2.5	0	2.5	0
CaAl	200	200	50	20	2.5	0	0	2.5
Placebo	200	000	00	20	5	0	0	0

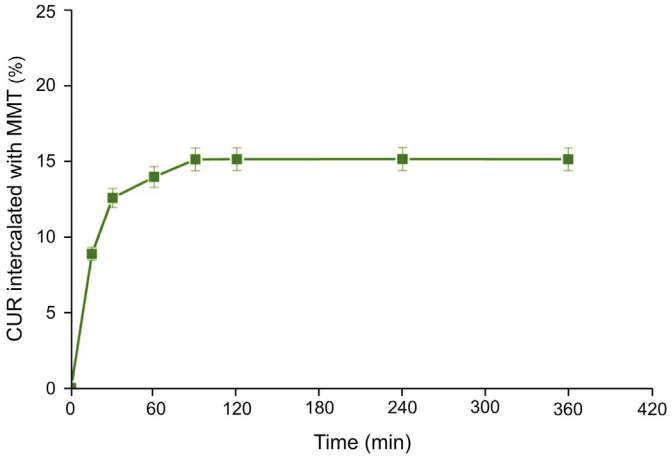

Fig. 2. Effect of time for intercalation of CUR with MMT.

2.3.6. Scanning electron microscopy (SEM)

The morphological characterization of microbeads was observed using SEM (JOEL MODEL JSM 840A) with an accelerated voltage of 20 kV equipped with an EDAX detector.

2.3.7. Swelling measurements

The swelling behaviour of different formulations was determined gravimetrically in simulated intestinal fluid (pH 7.4) and simulated gastric fluid (pH 1.2) at 37 °C. The percentage of equilibrium swelling degree was calculated using the following equation:

$$\text{Swelling degree } (\%) = \frac{W_s - W_d}{W_d} \times 100$$

Where W_s is the weight of swollen beads and W_d is the weight of dry beads.

2.4. Encapsulation efficiency (EE)

A known mass of drug loaded microbeads (40 mg) was immersed into 100 mL of phosphate buffer solution (pH 7.4, containing 5% absolute ethyl alcohol) for 24 h and then the suspension was agitated with an agate mortar to ensure the complete extraction of CUR from the microbeads and filtered through filter paper. The drug solution was analyzed by ultraviolet (UV) spectrophotometer (LabIndia, Mumbai, India) at the λ_{max} of 470.00 nm with placebo microbeads used as a blank correction. Concentration of drug was determined using calibration curve constructed by a series of CUR standard solutions. Percentage of EE was determined using the following formula.

$$\text{EE } (\%) = \frac{CUR_{added}\ (\text{mg}) - CUR_{free}\ (\text{mg})}{CUR_{free}\ (\text{mg})} \times 100$$

2.5. In vitro drug release studies

In vitro drug release studies of different formulations were carried out by using a dissolution tester (Lab India, Mumbai, India) containing eight baskets each with 900 mL of phosphate buffer solution (PBS) maintained at 37 °C, at a rotation speed of 50 rpm to replicate intestinal fluid (pH 7.4) and gastric fluid (pH 1.2)

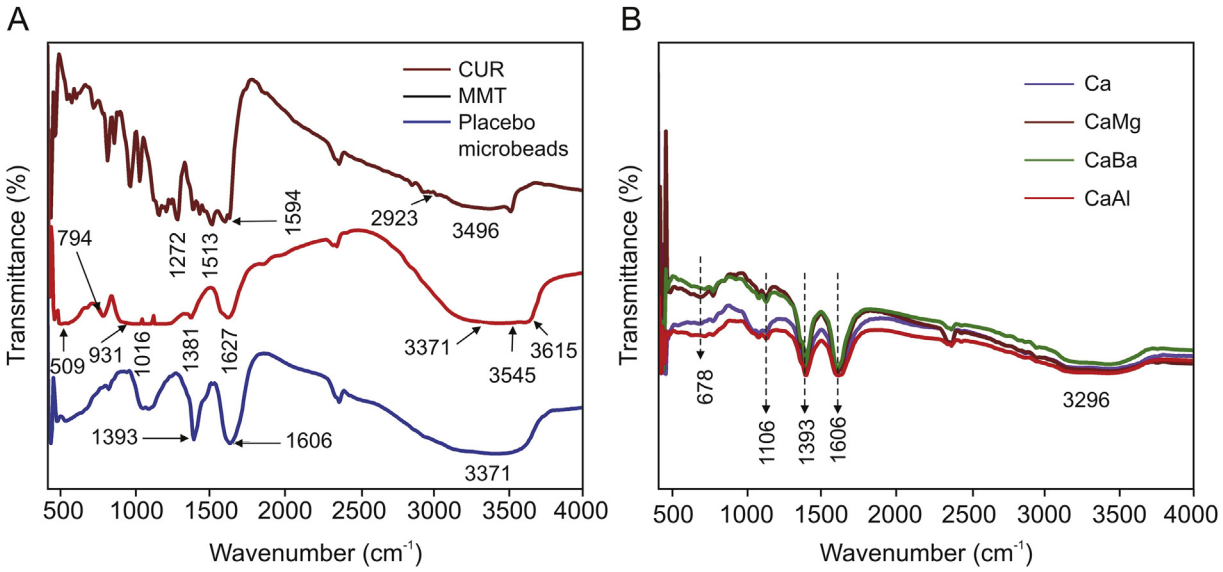

Fig. 3. FTIR spectrum of (A) CUR, MMT, placebo microbeads, and (B) drug SA/MMT loaded microbeads (Ca, CaMg, CaBa and CaAl).

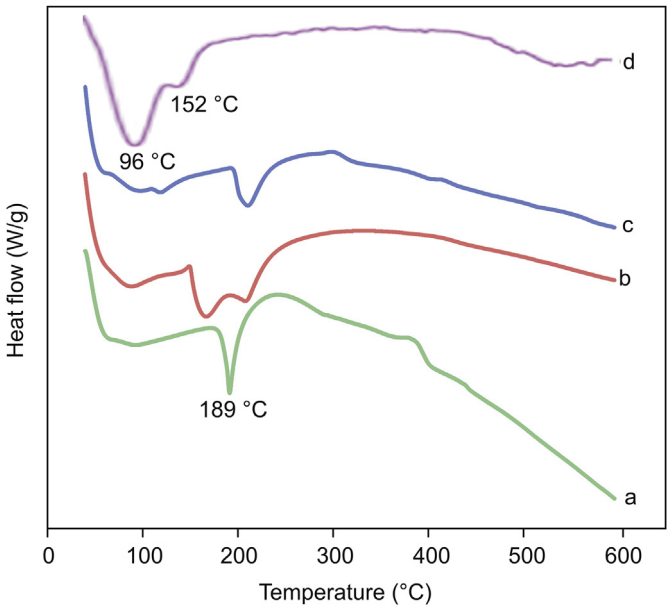

Fig. 4. DSC curves of (a) CUR, (b) placebo microbeads, (c) drug loaded SA/MMT microbeads (CaMg formulation) and (d) pristine MMT.

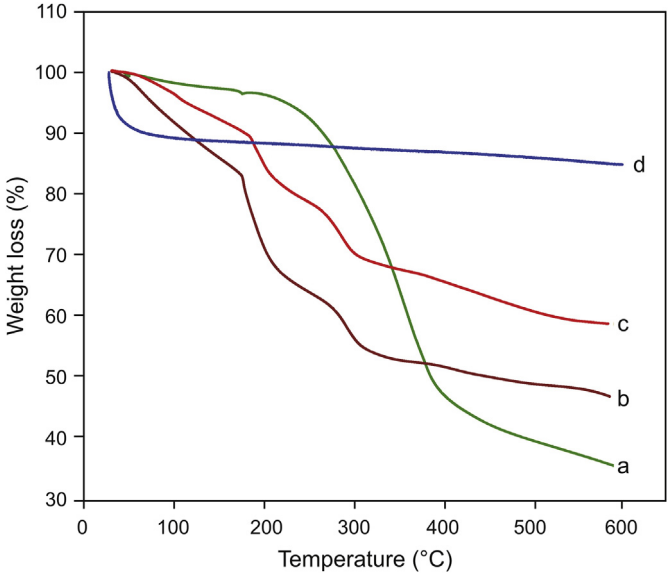

Fig. 5. TGA curves of (a) CUR, (b) placebo microbeads, (c) drug loaded SA/MMT microbeads (CaMg formulation) and (d) MMT.

atmosphere, respectively. 100 mg of the CUR loaded microbeads were taken in a dialysis bags for the drug release studies. At regular intervals of time, 5 mL aliquot samples were withdrawn, and analyzed using UV spectrophotometer at a fixed λ_{max} value of 470.00 nm, and the released drug amount was obtained by using concentration versus absorbance calibration curves. The withdrawn aliquot samples were replenished with equal volumes of PBS to simulate physiological conditions. The sink conditions were maintained throughout the release study.

3. Results and discussion

3.1. Intercalation kinetics

From Fig. 2, it was observed that 15.11% of CUR was intercalated with MMT electrostatically within 90 min and remained constant up to 360 min. Therefore, we should keep the time of 90 min for interaction between CUR and MMT to avoid partial interaction in the following experiments.

3.2. FTIR spectral analysis

The FTIR spectra of CUR, MMT, placebo microbeads, and drug loaded SA/MMT microbeads are presented in Fig. 3. The FTIR spectra of CUR show a characteristic broad peak at 3496 cm^{-1}, which corresponds to phenolic O–H stretching vibrations, a peak at 2923 cm^{-1} is assigned to aromatic C–H stretching vibrations, a peak at 1596 cm^{-1} corresponds to stretching vibration of benzene ring skeleton, a peak at 1513 cm^{-1} corresponds to mixed (C=O) and (C=C) vibration, a peak at 1272 cm^{-1} is assigned to Ar–O stretching vibrations. The FTIR spectra of MMT show distinct peaks at 3615 and 3545 cm^{-1} that are assigned to O–H stretching vibrations of Si–OH and Al–Al–OH, a peak at 3371 cm^{-1} corresponds to H–O–H stretching vibrations of interlayer water, a peak at 1627 cm^{-1} corresponds to H–O–H bending mode of adsorbed water, peaks at 1381, 1016 and 931 cm^{-1} correspond to (Si–O–Si) stretching frequency and peaks at 794 and 509 cm^{-1} are assigned to (O– Si–O) and (Al–Si–O) bending vibrations [28–30]. In case of placebo microbeads a peak at 3371 cm^{-1} is responsible for O–H stretching vibrations, a peak at 1616 cm^{-1} is assigned to C=O stretching vibrations, and a peak at 1393 cm^{-1} corresponds to COO- symmetric vibration. On comparing the drug loaded SA/MMT microbeads and pristine MMT, the Si–OH stretching of MMT at 3615 cm^{-1} disappeared in the spectra of drug SA/MMT microbeads, which confirmed that active sites of polymer matrix interacted with MMT. On comparing the placebo microbeads and drug loaded SA/MMT microbeads, the O–H stretching vibration of SA at 3371 cm^{-1} was shifted to lower side in dug loaded SA/MMT microbeads, which confirms that intermolecular hydrogen bonding takes place between polymer matrix and MMT clay [19]. And also a peak at 678 cm^{-1} indicates the presence of MMT composition in the matrix. The peak at 1616 cm^{-1} in placebo microbeads was shifted to 1606 cm^{-1} in drug SA/MMT loaded microbeads, which indicates that drug should have been loaded in the microbeads.

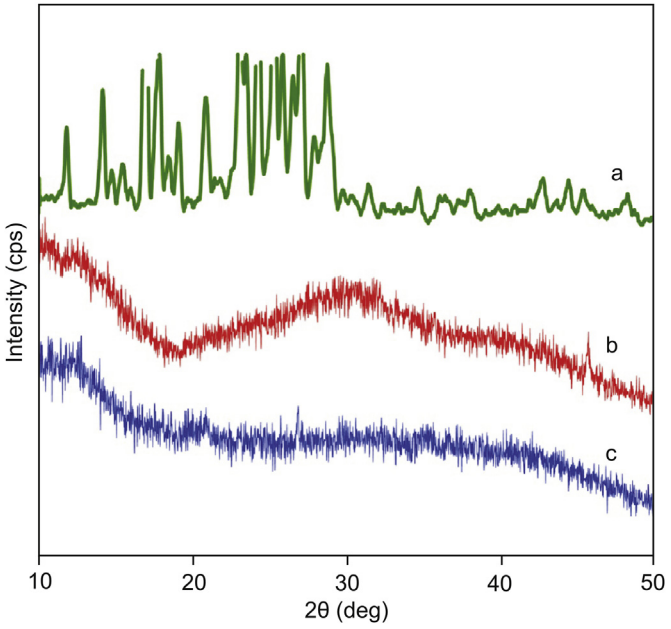

Fig. 6. X-RD patterns of (a) CUR, (b) placebo microbeads, and (c) drug loaded SA/MMT microbeads (CaMg formulation).

3.3. DSC analysis

To investigate the interaction of polymer matrix with MMT as well as crystalline nature of encapsulated CUR in the polymer matrix, DSC analysis was performed and the DSC curves are displayed in Fig. 4. The thermogram of placebo microbeads (Fig. 4b) shows a peak at 208 °C, whereas drug loaded SA/MMT microbeads (Fig. 4c) also showed the same peak as that of placebo microbeads but a slight variation was observed. And also another peak was observed in drug loaded SA/MMT microbeads at 164 °C. This confirmed that the interaction took place between active sites of polymer matrix and MMT, because MMT (Fig. 4d) also showed the same peak but a slight variation was observed. Fig. 4a shows a sharp peak at 189 °C for pure CUR, whereas such peak was not observed in drug loaded SA/MMT microbeads (Fig. 4c), which confirmed that the drug was molecularly dispersed in the microbeads.

3.4. TGA analysis

The TGA thermograms of CUR (a), placebo microbeads (b), drug loaded SA/MMT microbeads (c) and MMT (d) are displayed in Fig. 5. As shown in Fig. 5a, CUR should remain stable up to 169 °C; after that it followed mass loss and became maximum at 393 °C due to total degradation of the compound. In case of MMT (Fig. 5d), weight loss of 11% at 94 and 154 °C corresponds to dehydration of water molecules absorbed in pores and between the silicate layers [31], followed by weight loss of 4% in the region of 160–700 °C, corresponds to loss of structural water. The thermal decomposition of placebo microbeads (Fig. 5b) occurs in three consecutive steps. The first weight loss of 17% was found between 41 and 176 °C, which is ascribed to the evaporation of adsorbed water. The second weight loss step was observed between 180 and 299 °C with a loss of 23%, indicating the decomposition of the salt from the polymer network. The last step was observed in the region of 304–600 °C with a loss of 11% due to decomposition of polymer network which resulted in the formation of sodium carbonate [21]. In the case of drug loaded SA/MMT microbeads (Fig. 5c) four weight loss steps were observed. The first weight loss of 11% was observed in the region of 42–181 °C, followed by weight loss of 11% between the region of 185–254 °C due to degradation of CUR. The next two steps with weight loss of 10% and 17% were found in the region of 259–304 °C and 309–600 °C, which corresponds to decomposition of polymer network. The TGA results suggest that CUR loaded SA/MMT matrix showed an overall improvement in the thermal stability of microbeads.

3.5. X-RD analysis

To investigate the molecular dispersion of CUR in polymer matrix, X-RD analysis was performed and the diffractograms of CUR (a), placebo microbeads (b) and CaMg microbeads (c) are presented in Fig. 6. The diffractogram of CUR (Fig. 6a) shows characteristic peaks in the 2θ region of 12-28° because of its crystallinity. However, these characteristic peaks disappeared in drug loaded SA/MMT microbeads (Fig. 6c), which indicates that the CUR changes its state from crystalline to amorphous nature. These results suggest that CUR was molecularly dispersed in the polymeric network.

3.6. SEM analysis

To study the morphology of microbeads, SEM analysis was performed and the topographical images are displayed in Fig. 7. From Fig. 7, it can be clearly observed that the microbeads have rough surface with visible wrinkles. In all formulations it was

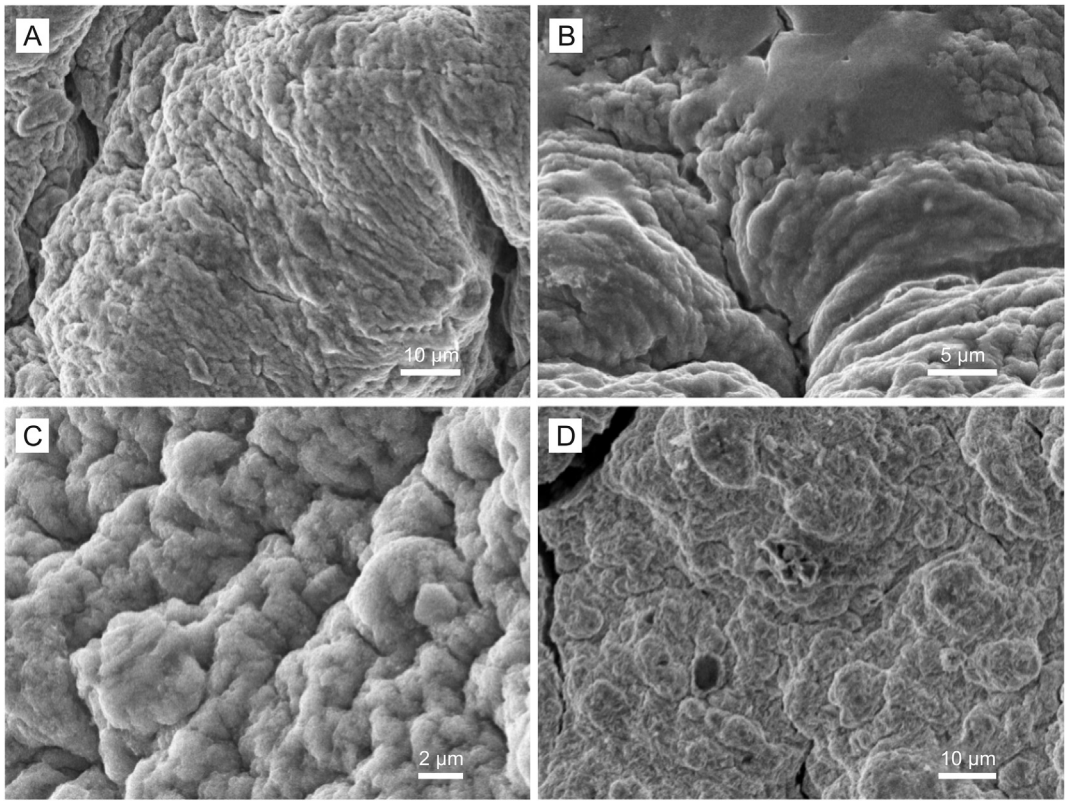

Fig. 7. SEM images show effect of MMT and divalent ions on polymer network: (A) Ca, (B) CaMg, (C) CaBa and (D) CaAl.

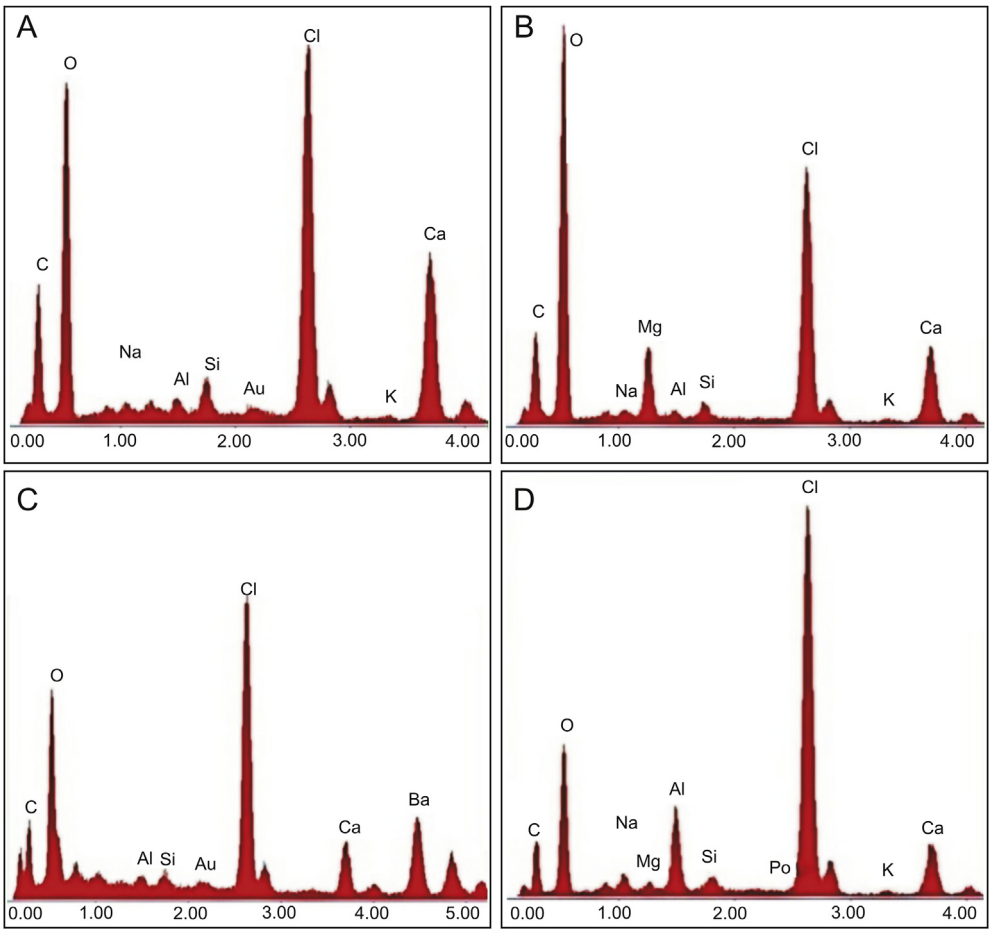

Fig. 8. EDS spectra of (A) Ca, (B) CaMg, (C) CaBa and (D) CaAl.

observed that high roughness is present, which indicates the presence of MMT platelets on outer surface of microbeads. On comparing the Ca (Fig. 7A) and CaMg (Fig. 7B) formulations, more porous nature was observed in CaMg than in Ca. The porous nature is due to the presence of Mg^{2+} cations in the network, which forms less rigid structure. The reason is that Mg^{2+} ions are less strongly coordinated with the alginate than Ca^{2+} ions and therefore more porous nature was observed. This was further correlated with the swelling and drug release studies. A similar observation was reported by Sanchez-Ballester et al. [18]. In contrast, the formulations CaBa (Fig. 7C) and CaAl (Fig. 7D) show less porous nature, which is due to formation of more rigid structure. From the results of SEM images, the average size of microbeads was found to be 800–1100 μm.

3.7. Energy-dispersive X-ray spectra (EDS) analysis

To evaluate the elemental composition of Ca, CaMg, CaBa and CaAl microbeads, EDS analysis was performed and their spectra are presented in Fig. 8. From Fig. 8, it can be clearly observed that in all formulations Al and Si peaks were observed, which confirmed that MMT presented in all formulations. EDS spectra of CaMg, CaBa and CaAl show Mg, Ba and Al peaks, respectively. This confirmed that multivalent ions were incorporated in the calcium alginate network.

3.8. Swelling measurements

Swelling degree is one of the important factors of SA beads for control release in drug delivery systems [32]. In order to determine the swelling degree of all formulations, swelling experiments were performed in simulated intestinal fluid (pH 7.4) and simulated gastric fluid (pH 1.2) at 37 °C and the results are presented in Fig. 9. From Fig. 9, it is clearly observed that the swelling degree is more at pH 7.4 than at pH 1.2. Therefore, SA beads are good promising carriers to deliver drug molecules in the intestines and to avoid gastric release of drugs.

From Fig. 9 it is observed that the swelling degree of all formulations differed based on the amount of multivalent ions present in the beads. The maximum swelling degree of all profiles was observed at 60 min and thereafter slightly decreased. On comparing all the formulations, CaMg beads showed high percentage of water uptake because the Mg^{2+} ions formed less rigid network than the all other formulations; therefore, the water molecules entered the beads through the pores; thereby the percentage of swelling increased. On the other hand, the CaBa and CaAl showed less percentage of water uptake because the Ba^{2+} and Al^{3+} formed a tight rigid network, such that the polymer network was unable to allow a large number of water molecules, so the swelling decreased.

3.9. Encapsulation efficiency (EE)

The EE of CUR varied for all formulations depending on the presence of multivalent ions in beads and the results are listed in Table 2. The EE decreased in CaBa and CaAl formulations, because the network structure of these formulations was more rigid, thereby swelling to less extent, which resulted in low EE values. In Ca and CaMg formulations, the EE increased because it formed less

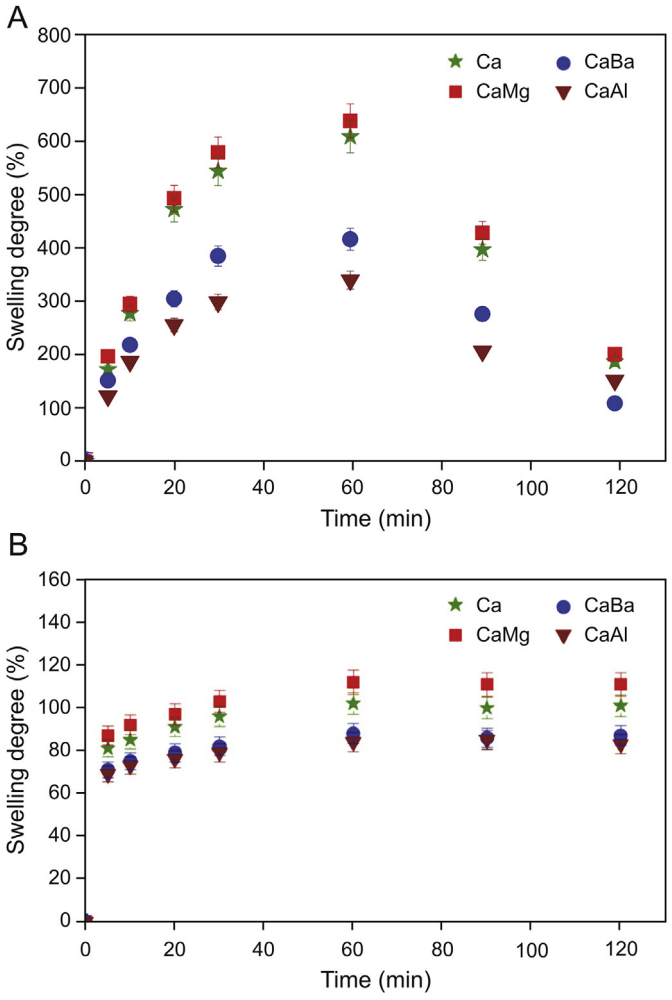

Fig. 9. Swelling studies of Ca, CaMg, CaBa and CaAl at (A) pH 7.4 and (B) pH 1.2 at 37 °C.

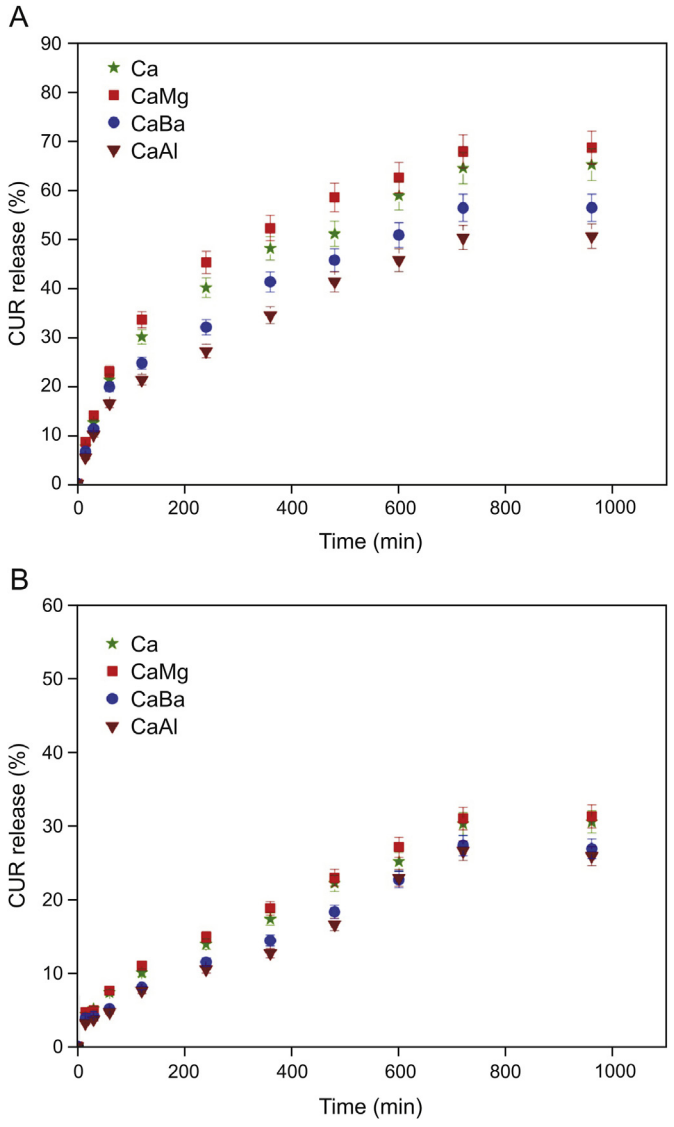

Fig. 10. CUR release of Ca, CaMg, CaBa and CaAl at (A) pH 7.4 and (B) pH 1.2 at 37 °C.

rigid network, thereby swelling to more extent, which resulted in high EE values.

3.10. In vitro drug release studies

The in vitro release studies were carried out in simulated intestinal fluid (pH 7.4) and simulated gastric fluid (pH 1.2) at 37 °C and the results are displayed in Fig. 10. From Fig. 10, it is observed that the release rate is higher at pH 7.4 than at pH 1.2, because at pH 7.4 the carboxylic groups show less interactions with buffer media, allowing the network to be more loose; hence the entrapped drug molecules easily leaches out from the network. From Fig. 10, it is observed that similar to swelling behaviour, in vitro release rate also shows the same type of results. In the case of Ca and CaMg profiles, CaMg shows high release than Ca, which is due to its more porous structure and also formation of weaker interaction between Mg^{2+} ions and alginates. This would contribute to CaMg beads' disintegrating more readily in the dissolution medium and drug molecules easily leach out from the polymer matrix, whereas in the case of CaBa and CaAl the drug release rate decreases because it forms more rigid structure; hence CUR molecules have less chance to escape out from the matrix.

The obtained in vitro drug release data of CUR loaded microbeads at pH 7.4 were fitted into different mathematical

Table 2
Release kinetics parameters at pH 7.4 and encapsulation efficiency (EE) of all samples.

Formulation code	Korsmeyer Peppas		Higuchi		First		Zero		EE (%)
	r^2	n	r^2	k	r^2	k	r^2	k	
Ca	0.926	0.550	0.987	2.028	0.932	1.921	0.916	15.225	62.43
CaMg	0.980	0.572	0.982	2.016	0.916	1.906	0.893	17.471	66.21
CaBa	0.962	0.550	0.983	2.017	0.925	1.932	0.935	12.920	58.64
CaAl	0.957	0.551	0.990	2.027	0.930	1.944	0.952	10.545	55.40

models such as zero order, first order and Higuchi. The release rate constant and correlation coefficient of all formulations are shown in Table 2. The correlation coefficient values of CUR loaded microbeads followed neither zero order nor first order, but the correlation coefficient values were close to the Higuchi model. Therefore, the drug release kinetics of CUR loaded microbeads followed Higuchi model. According to Higuchi model, the release of drug from the microbeads involves the penetration of liquid into the matrix and dissolving of the drug, which then diffuses the drug into the exterior liquid through pores or intestinal channels. However, this type of phenomenon is observed in hydrophilic matrix system. Therefore, the drug release rate of CUR loaded microbeads shows the phenomenon of swelling and erosion of the polymer simultaneously.

To understand the drug release mechanism, the data obtained from in vitro drug release studies in PBS (7.4) were fitted into the following Korsmeyer-Peppas equation [33].

$$\frac{M_t}{M_\alpha} = \mathrm{kt}^{\mathrm{n}}$$

Where, M_t is the cumulative release of CUR at time t, M_α is the total amount of CUR in the matrix, k is a characteristic release constant of the drug-polymer system and n is the release exponent indicating the type of drug release mechanism. The results of n and k are listed in Table 2. For spherical drug carriers, if $n < 0.43$, the drug diffuses from the polymer matrix according to Fickian diffusion; if $0.43 < n < 0.85$, anomalous or non-Fickian type drug diffusion occurs; if $n = 0.85$, Case-II kinetics is operative; if $n > 0.85$, the mode of drug release follows the super Case-II diffusion. In the present data n values were obtained in the range of 0.550–0.572, which indicates non-Fickian type of diffusion process.

4. Conclusion

In the present work, dual cross-linked SA/MMT microbeads were fabricated by ionotropic gelation method for the extended release of CUR. FTIR confirmed the interaction between drug molecules and polymer network. DSC, TGA and X-RD studies confirmed the chemical stability and molecular level dispersion of CUR in microbeads, respectively. SEM studies confirmed the presence of MMT platelets on the outer surface of microbeads. The effect of the incorporation of multivalent ions on crosslinking of SA chains, swelling studies and drug release studies were thoroughly examined. The CaMg beads showed highest percentage of water uptake at pH 7.4 compared to other formulations due to the formation of less rigid network, whereas the CaAl beads showed less percentage of water uptake due to the formation of tight rigid network. The drug release profiles at pH 7.4 were correlated with the swelling results, and the CaMg and CaAl beads showed the highest and lowest drug release rates, respectively. The in vitro results were fitted into peppas equation and the results showed that the drug mechanism followed non-Fickian type of diffusion process. Based on all these results, the developed microbeads are considered to be potentially good drug carriers for extended release of CUR.

Declaration of competing interest

The authors declare that there are no conflicts of interest.

Acknowledgments

The authors C. Madhavi and K. Chowdoji Rao thank UGC–BSR, New Delhi, India, for the financial support provided.

Appendix A. Supplementary data

Supplementary data to this article can be found online at https://doi.org/10.1016/j.jpha.2020.07.002.

References

[1] S. Ganguly, P.P. Maity, S. Mondal, et al., Polysaccharide and poly(methacrylic acid) based biodegradable elastomeric biocompatible semi-IPN hydrogel for controlled drug delivery, Mater. Sci. Eng. C 92 (2018) 34–51.
[2] K. Varaprasad, G.M. Raghavendra, T. Jayaramudu, et al., A mini review on hydrogels classification and recent developments in miscellaneous applications, Mater. Sci. Eng. C 79 (2017) 951–978.
[3] X. Sun, J. Shi, X. Xu, et al., Chitosan coated alginate/poly(N isopropylacrylamide) beads for dual responsive drug delivery, Int. J. Biol. Macromol. 59 (2013) 273–281.
[4] I. Constantinidis, S.C. Grant, S. Celper, et al., Non-invasive evaluation of alginate/poly-l-Lysine/Alginate microcapsules by magnetic resonance microscopy, Biomaterials 28 (2007) 2438–2445.
[5] M.I. Carretero, M. Pozo, Clay and non-clay minerals in the pharmaceutical industry: Part I. Excipients and medical applications, Appl. Clay Sci. 46 (2009) 73–80.
[6] S. Hua, H. Yang, A. Wang, A pH-sensitive nanocomposite microsphere based on chitosan and montmorillonite with in vitro reduction of the burst release effect, Drug Dev. Ind. Pharm. 36 (2010) 1106–1114.
[7] R.I. Iliescu, E. Andronescu, C.D. Ghitulica, et al., Montmorillonite-alginate nanocomposite as a drug delivery system-incorporation and in vitro release of irinotecan, Int. J. Pharm. 463 (2014) 184–192.
[8] J. Choy, S. Choi, J. Oh, et al., Clay minerals and layered double hydroxides for novel biological applications, Appl. Clay Sci. 36 (2007) 122–132.
[9] Y. Huang, Q. Tao, D. Hou, et al., A novel ion-exchange carrier based upon liposome-encapsulated montmorillonite for ophthalmic delivery of betaxolol hydrochloride, Int. J. Nanomed. 12 (2017) 1731–1745.
[10] V.V. Krupskaya, S.V. Zakusin, E.A. Tyupina, et al., Experimental study of montmorillonite structure and transformation of its properties under treatment with inorganic acid solutions, Minerals 7 (2017) 49–63.
[11] T. Li, L. Zhao, Z. Zheng, et al., Design and preparation acid-activated montmorillonite sustained-release drug delivery system for dexibuprofen in vitro and in vivo evaluations, Appl. Clay Sci. 163 (2018) 178–185.
[12] V. Anand, R. Kandarapu, S. Garg, Ion-exchange resins: carrying drug delivery forward, Drug Discov. Today 6 (2001) 905–914.
[13] C. Aguzzi, P. Cerezo, C. Viseras, et al., Use of clays as drug delivery systems: possibilities and limitations, Appl. Clay Sci. 36 (2007) 22–36.
[14] K.M. Reddy, V.R. Babu, K.S.V.K. Rao, et al., Temperature sensitive semi-IPN microspheres from sodium alginate and N-isopropylacrylamide for controlled release of 5-fluorouracil, J. Appl. Polym. Sci. 107 (2008) 2820–2829.
[15] P.R.S. Reddy, K.M. Rao, K.S.V.K. Rao, et al., Synthesis of alginate based silver nanocomposite hydrogels for biomedical applications, Macromol. Res. 22 (2014) 832–842.
[16] T. Wu, J. Huang, Y. Jiang, et al., Formation of hydrogels based on chitosan/alginate for the delivery of lysozyme and their antibacterial activity, Food Chem. 240 (2017) 361–369.
[17] G.T. Grant, E.R. Morris, D.A. Rees, et al., Biological interactions between polysaccharides and divalent cations: the egg-box model, FEBS Lett. 32 (1973) 195–198.
[18] N.M. Sanchez-Ballestera, I. Soulairola, B. Bernard, et al., Flexible heteroionic calcium-magnesium alginate beads for controlled drug release, Carbohydr. Polym. 207 (2019) 224–229.
[19] B.D. Kevadiya, G.V. Joshi, H.A. Patel, et al., Montmorillonite-alginate nanocomposites as a drug delivery system: intercalation and in vitro release of Vitamin B1 and Vitamin B6, J. Biomater. Appl. 25 (2010) 161–177.
[20] H. Bera, S.R. Ippagunta, S. Kumar, et al., Core-shell alginate-ghatti gum modified montmorillonite composite matrices for stomach-specific flurbiprofen delivery, Mater. Sci. Eng. C 76 (2017) 715–726.
[21] S. Jain, M. Datta, Montmorillonite-alginate microspheres as a delivery vehicle for oral extended release of Venlafaxine hydrochloride, J. Drug Deliv. Sci. Technol. 33 (2016) 149–156.
[22] K.M. Rao, K.S.V.K. Rao, G. Ramanjaneyulu, et al., Curcumin encapsulated pH sensitive gelatin based interpenetrating polymeric network nanogels for anti cancer drug delivery, Int. J. Pharm. 478 (2015) 788–795.
[23] E.S. Behbahani, M. Ghaedi, M. Abbaspour, et al., Curcumin loaded nanostructured lipid carriers: in vitro digestion and release studies, Polyhedron 164 (2019) 113–122.
[24] J. Sun, C. Bi, H.M. Chan, et al., Curcumin-loaded solid lipid nanoparticles have prolonged in vitro antitumour activity, cellular uptake and improved in vivo bioavailability, Colloids Surf. B: Biointerfaces 111 (2013) 367–375.
[25] H.W. Chen, H.C. Huang, Effect of curcumin on cell cycle progression and apoptosis in vascular smooth muscle cells, Br. J. Pharmacol. 124 (1998) 1029–1040.
[26] S. Kar, B. Kundu, R.L. Reis, et al., Curcumin ameliorates the targeted delivery of methotrexate intercalated montmorillonite clay to cancer cells, Eur. J. Pharmaceut. Sci. 135 (2019) 91–102.
[27] H.H. Tonnesen, J. Karlsen, Studies on curcumin and curcuminoids. VI. Kinetics

of curcumin degradation in aqueous solution, Z. Lebensm. Unters. Forsch. 180 (1985) 402–404.
[28] H.A. Patel, R.S. Somani, H.C. Bajaj, et al., Preparation and characterization of phosphonium montmorillonite with enhanced thermal stability, Appl. Clay Sci. 35 (2007) 194–200.
[29] R. Abdeen, N. Salahuddin, Modified chitosan-clay nanocomposite as a drug delivery system intercalation and in vitro release of ibuprofen, J. Chem. (2013), 576370.
[30] M.A. Guler, M.K. Gok, A.K. Figen, et al., Swelling, mechanical and mucoadhesion properties of Mt/starch-g-PMAA nanocomposite hydrogels, Appl. Clay Sci. 112–113 (2015) 44–52.
[31] X. Zheng, J. Dou, J. Yuan, et al., Removal of Cs^{+} from water and soil by ammonium-pillared montmorillonite/Fe3O4 composite, J. Environ. Sci. 56 (2007) 12–24.
[32] P. Del Gaudio, P. Colombo, G. Colombo, et al., Mechanisms of formation and disintegration of alginate beads obtained by prilling, Int. J. Pharm. 302 (2005) 1–9.
[33] K.S.V.K. Rao, Ildoo Chung, K.M. Reddy, et al., PMMA-based microgels for controlled release of an anticancer drug, J. Appl. Polym. Sci. 111 (2009) 845–853.